Seismic performance characterization of Nepali school buildings using a novel micro-modeling approach

By

© 2021

Alok Bhatta

B.S. Tribuwan University, 2016

Submitted to the graduate degree program in Civil, Environmental and Architectural Engineering and the Graduate Faculty of the University of Kansas in partial fulfillment of the requirements for the degree of Master of Science in Civil Engineering

_____

Chair: Elaina Sutley, Ph.D.

_____

Jian Li, Ph.D., P.E.

_____

Rémy Lequesne, Ph.D., P.E.

_____

Michael Taylor, Ph.D.

Date Defended: 7 May 2021

The thesis committee for Alok Bhatta certifies that this is the approved version of the following thesis:

Seismic performance characterization of Nepali school buildings using a novel micro-modeling approach

Chair: Elaina Sutley, Ph.D.

Date Approved: May 12, 2021

Abstract

The ultimate goal of this research is to reduce the seismic vulnerability of school buildings in rural Nepal. Following the 2015 Gorkha earthquake in Nepal, major changes were adopted into seismic design code provisions regarding school construction. Perhaps the most significant change was an intention to regulate school building construction. While seismic design provisions and regulating building practices is a positive step forward, the seismic performance of school buildings built to the newer standards was unknown, or at least not available in the literature. This thesis aims to fill this gap in knowledge by applying a novel micro-modeling approach to developing a finite element model of a rural school building of stone in mud masonry construction typology. The thesis starts by setting the context and high-level motivation for the problem. The foundation of research which this work builds upon is then presented. The construction characteristics of the building typology described above is presented in detail, as well as how structural and material parameters required for the nonlinear dynamic analysis are derived or otherwise obtained. The modeling approach is presented with a description of the wall systems which use a 3D computational method using homogenization for the analysis of general heterogenous thick shell structures. Finally, seismic performance assessment using seven regionally-relevant seismic ground motions is conducted for the modeled building using Incremental Dynamic Analysis. Fragility functions are derived from the IDA results, and used to characterize and discuss the seismic performance of the school building. While more work is needed in this area, this thesis can be used to understand the associated seismic risk of the new designs mandated for school buildings constructed in rural Nepal.

Acknowledgements

This research was supported by the National Science Foundation (NSF Award No. 1827866). Any opinions, findings, and conclusions or recommendations expressed in this material are those of the authors and do not necessarily reflect the views of the NSF.

The research was carried out in Department of Civil, Environmental, and Architectural Engineering at the University of Kansas. I am very grateful to the University for providing me with the space and resources to successfully carry out this research. I wish to express my profound gratitude to the members of dissertation committee, namely, Professors Elaina J. Sutley, Remy D. Lequesne, Jian Li, and Michael Taylor for their invaluable comments and suggestions.

I am extremely grateful to my academic advisor, Professor Elaina J. Sutley for advising me through my graduate study and providing me necessary guidance and training to successfully finish my study at the University of Kansas. Her continuous and ever-present support contributed significantly to my understanding about the subject matter.

TABLE OF CONTENTS

Page

1 INTRODUCTION..... 1

2 LITERATURE REVIEW..... 8

2.1 Nepal's Seismic and Cultural Context 8

2.2 Review of Building Specifications and Code Regulations 10

2.3 Damage Assessment Reports After 2015 Gorkha Earthquake 14

2.4 Experimental Investigations on Building Materials and Specifications 15

2.4.1 Static Loading Tests on Stone or Mortar Units and Wall Specimens 16

2.4.2 Shake Table Tests of Stone Masonry Type Buildings Built in Mud-Mortar 18

2.5 Experimental Investigations on Seismic Provisions and Retrofitting Strategies 20

2.6 Numerical Investigations of Nepalese Structures 23

3 METHODOLGY 29

3.1 Introduction to the Numerical Model used in the Analysis 29

3.2 Selected Case Building and Specifications 31

3.3 Selection of Seismic Sources and Ground Motions 34

3.4 Proposed Criteria for the Definition of Suitable Limit States 37

3.5 Nonlinear Dynamic Analysis Specifications 38

3.6 IDA and Fragility Curve Development 40

4 RESULTS AND DISCUSSION 42

4.1 Limit States and Failure Modes 42

4.2 Incremental Dynamic Analysis (IDA) Curve and Fragility Analysis 45

5 CONCLUSION 48

REFERENCES 52

1 Introduction

The objectives of this thesis are to (1) build high-fidelity models of present designs of rural Nepali school buildings, (2) simulate a series of relevant seismic excitations, and (3) quantify the seismic performance of the recent structural design changes. Empirical studies are available for residential buildings common in rural Nepal, albeit in limited quantity; however, reliable models for predicting school buildings' fragility remain a major gap in the literature (Gautam et al., 2018; Didier et al., 2017). Given the international attention garnered around the rebuilding and replacement of school buildings after the major 2015 Gorkha earthquake, a reliable and quantitative understanding of school building seismic performance is very important. This project contributes new knowledge towards the seismic evaluation of unreinforced masonry (URM) buildings using stone with mud mortar construction; the most common structural wall system for rural school buildings in Nepal (Giordano et al., 2021).

Nepal lies in an active seismic zone formed due to subduction of the Indian and Eurasian plate, making it vulnerable to extensive seismic activity. Specifically, Nepal is divided into three tectonic zones from south to north, viz., the Main Central Thrust (MCT), the Main Boundary Thrust (MBT), and the Main Frontal Thrust (MFT), with major and minor recent earthquakes associated with these active thrusts. The 1934 earthquake (M_w 8.4) is the highest recorded ground motion in Nepal's history; high-intensity earthquakes have been recorded every seven to eight decades since 1255 AD (Chaulagain et al., 2016). The most recent catastrophic earthquake was the 2015 Gorkha M_w 7.8 mainshock with an epicenter in the Barpak village of the Gorkha district, around 76 km northwest from the capital city of Kathmandu (USGS, 2015). The earthquake occurred near the MFT, due to the subduction action of plates moving at a relative rate of approximately 45 mm/year (USGS, 2015). Approximately 260 aftershock events with a

magnitude M_L greater than 4.0 occurred in the following months after the mainshock. The 2015 Gorkha earthquake and its many aftershocks caused more than 9,000 fatalities, 25,000 injuries, critically damaged more than 800,000 homes, and destroyed more than 7,550 schools (NPC, 2015).

After the 2015 earthquake and aftershocks subsided, reconstruction began and was led primarily by the Nepal Reconstruction Authority (NRA) in coordination with other international agencies (NPC, 2015). In 2016, "Seismic Retrofitting Guidelines in Nepal" was published for adobe structures, masonry structures, and reinforced concrete (RC) structures covering both theoretical and practical aspects of new construction guidelines, which has been pivotal in the reconstruction process of school buildings (CoRD, 2016). School buildings in rural Nepal are historically constructed using stone units and mud mortar wall assemblies and account for almost 85% of the total building types, as seen from Fig. 1. Generally, stones or bricks are used as wall units with mud mortar or cement mortar as binding agents. Approximately 42% of school buildings have mud bonded bricks or stone exterior walls, and approximately 29% of exterior walls are built with cement bonded bricks or stone; the remaining 29% use bamboo or wood (CBS, 2012).

Almost 95% of school buildings are low-rise buildings, specifically one to two stories (Giordano et al., 2021). Hence, the selection for this thesis is narrowed down to low-rise stone masonry buildings in mud-mortar as the representative typology of rural school buildings.

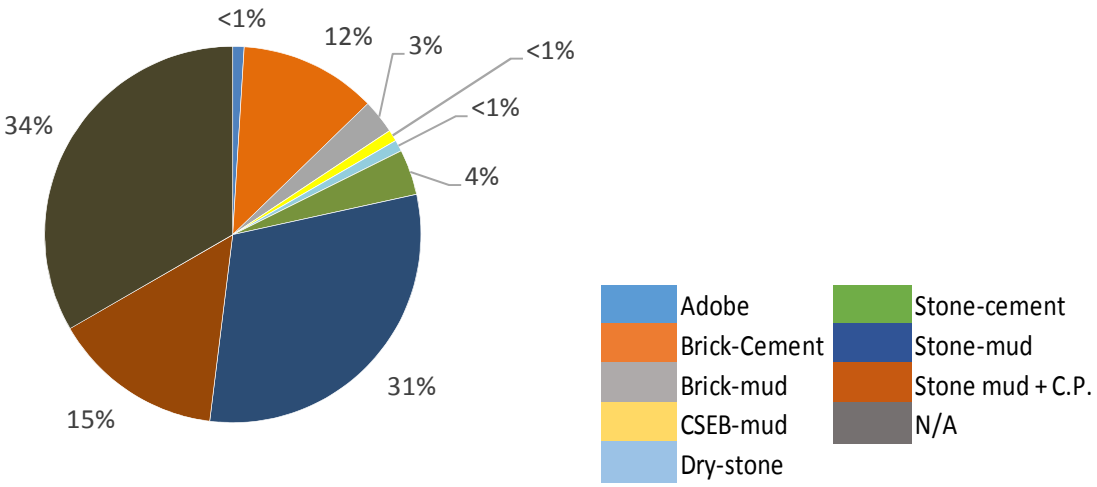

Fig. 1. Percentage distribution of structural typology of Nepali school buildings (Modified from Giordano et al., 2021)

While the first official building codes in Nepal were published in 1994 (NBC, 1994), there is evidence that the regulatory mechanisms were more closely and consistently followed and inspected only after the 2015 Gorkha earthquake (NPC, 2015). Modern designs continue to use stone units and mud mortar wall assemblies, but now incorporate wood lentil bands into the wall system, among other structural provisions, and the roof system is comprised of wood trusses supporting a metal roof membrane (see Fig. 2). These changes decreased the weight and increased the flexibility of the buildings, however, their true improvement to the building's seismic performance has not been quantified. In both cases, material property and structural characterization have high variability; materials are extracted local to the site and thus vary across Nepal. Accurately modeling building parameters, and validating the resulting models are major challenges for this research.

Fig. 2. Typical school building built with stone masonry walls in cement mortar with metal roof (Image credit: Dr. Elaina J. Sutley)

It should be highlighted that most of the structural deficiencies in stone masonry buildings were caused due to a lack of proper reinforcement in different structural members and poor connections between these members; delamination is also caused as a result of the lack of homogeneity between the stone and mortar units (Gautam et al. 2016). However, it is important to ensure that the recent steps taken towards better construction practices of Nepal are based on a learned and well-researched foundation. The availability of fast computational abilities and reliable modeling methods is no longer a constraint to designing sophisticated structural engineering models for common building typologies present in Nepal. The three commonly pursued methods for seismic evaluation of buildings are a) empirical method, broadly, based on seismic damage types from observed field assessments, as adopted in Gautam et al. (2018), b) analytical methods which involves solving a constitutive equation on finite modeling of wall elements or other homogenization techniques, as in Petracca (2016) and c) experimental tests

conducted on single-wall specimens using static loading or full-scale shake table tests to obtain material parameters for the seismic evaluation and also as verification of the analytical model. These investigations are discussed briefly here, and in detail in Chapter 2.

Empirical evaluation is based on field observations of various damage modes, categorizing said modes into corresponding damage states, and producing empirical fragility functions. Following the 2015 Gorkha earthquake sequence, Global Program for Safer Schools (GPSS) trained 150 engineers to conduct observational damage assessments for 18,000 school buildings across affected districts. The results of this assessment were incorporated into a database which was then analyzed in Giordano et al. (2021) to identify primary structural characteristics and failure modes of the Nepalese building stock. Empirical studies can help document what went wrong with previous design and construction approaches but are limited in their ability to advance design given that component-level loading cannot be obtained, material properties cannot be directly obtained, and failure sequence of the structural system is often difficult to determine.

Analytical studies present an opportunity to simulate different loads, and to model and measure component and system behavior to advance design. Analytical studies depend on experimental investigations for material parameter inputs through static or shake table tests that are subjected to different types of loading to obtain average material properties. However, there is a high degree of uncertainty in numerical modeling due to the record-to-record variability of ground motions, the analytical methodology, the uncertainty in the materials and geometric properties of different building typologies, and the definition of the damage states.

Experimental tests are generally limited because they must be done at the component level to save cost, or if done at the system level as in full-scale shake table testing, then typically only

one specimen is examined. Some relevant experiments to determine material properties for the stone and mud mortar assemblies for Nepal's context are referenced and detailed in the following chapters. Given limitations of all three seismic evaluation approaches, this study adopted an analytical approach as the primary investigation tool and references the experimental works of others for parametric values.

The analytical results presented in Chapter 4 of this thesis are validated using findings from empirical studies after the 2015 earthquake, and with comparisons to standardized design calculations. The building models were developed in Scientific Toolkit for OpenSees (STKO) using a micro-modeling approach characterized by a nonlinear mortar interface, capable of satisfactorily representing the shear behavior of mortar joints. STKO provides an excellent platform for analyzing detailed micromodels for materials such as masonry. Masonry is complex to model because it is initially orthotropic, and as the damage evolves it becomes anisotropic (Petracca, 2016). As masonry is composed of large components like stone and mortar joints, and with the non-periodic unit arrangement, micro modeling is necessary. The micro model captures all applicable failure mechanisms and the analysis remains stable until collapse, at which point the iteration fails to converge.

To better understand the seismic performance of the building models for different suites of ground motions, an Incremental Dynamic Analysis (IDA) is adopted. IDA involves subjecting the modeled structure to multiple accelerogram records, each set to incremental levels of intensity by introducing a simple transformation by scaling up or down the amplitudes (Vamvatsikos et al. 2002). The selection and application of ground motion conditions are sensitive to the reliability of the overall analysis. The ground motions used for this study were obtained from the PEER NGA database portal based on earthquake parameters derived from

disaggregated data from some of the major fault systems of Nepal, obtained from Stevens et al. (2018). The results of the IDA are used to produce fragility functions, which are the probability of non-exceedance for specific peak ground accelerations, for the building models.

The motivation leading up to this project and the overview of the thesis is presented in this chapter, by identifying current practices of stone masonry building construction, and the vulnerability associated with school buildings. The remaining chapters are organized as follows: Chapter 2 provides a literature review of relevant research methodologies and findings useful for verification purposes. In Chapter 3, the research methodology is presented based on the school building typology used in the seismic evaluation, with the results based on elastic and inelastic properties and the arrangement/ periodicity of units, with which all variations of failure mechanisms can be observed. Chapter 4 presents the micro model of the school building, findings from the Incremental Dynamic Analysis, and subsequent fragility curves. This thesis concludes with some recommendations for better seismic resiliency of stone masonry building types in general, and suggestions for continued investigation to support safer building techniques.

2 Literature Review

2.1 Nepal's Seismic and Cultural Context

Although Nepal is a relatively small country compared to its two neighboring giants, India and China, it has a wide range of geographical variations from the highest mountains in the world to the plains in the south. The housing typology differs according to the location and so do construction practices. More than 60% of Nepalese construction is in rural areas (Chaulagain et al. 2016). Poor-conditioned road networks that can be completely washed out during the annual monsoon season and covered with snow in winter, and local economic hardships, make it a challenge for people in the rural areas to choose quality construction materials (LBJ, 2018).

Nepal's rural population continues to face economic hardships due to a lack of road networks and other basic amenities. Lack of stability in governance in conjunction with unfavorable topography hinders the development of various infrastructures, with corruption being rampant at the governmental level (Gautam et al., 2020). Among Nepal's total population of 28 million, 8 million are said to be below the poverty line, which is 33% of the total rural population and only 7% of the total urban population (Multidimensional Poverty Index, 2018). The devastation caused by the 2015 Gokha earthquake, particularly the rural housing settlements, worsened living conditions for people who were struggling to meet their basic needs. Natural building materials like stone, mud, timber, and bamboo minimize the cost of construction for school building construction, as most are locally available in surrounding forests and river beds. Hence, it would be highly beneficial to improve the viability of locally available materials in any structural advancements proposed for school or residential buildings in remote parts of Nepal.

Unreinforced masonry (URM) is the most adopted construction type in Nepal, both before and after the 2015 Gorkha earthquake (CBS, 2012). The scenario of residential buildings can be an important reflection of the overall building practices in rural Nepal. There is a significant variation of URM construction in Nepal, ranging from roofing styles to exterior walls.

According to NSET (2000), the trend of poor construction practice is prevalent in the construction of school buildings. Before 2015, school buildings in rural areas were primarily built by local masons who were almost always trained only with local construction techniques and did not incorporate seismic provisions in construction practices. The lack of proper technical supervision was owed to the difficult road accessibility in these areas, as a result, a major part of the rural Nepalese housing stock did not follow standardized engineering guidelines either. Many older school buildings also suffered from a lack of maintenance, and had softened through the years through past earthquakes and lack of repair, altogether creating a vulnerable landscape for the 2015 earthquake.

The role of school buildings can be much important in terms of providing immediate shelters, and for emergency rescue operations, as seen in the 2015 earthquake (NPC, 2015). Since the 2015 earthquake, there have been few positive changes in the existing building codes or retrofitting guidelines, and also in the implementation guidelines (CoRD, 2016). Of the changes that were made, it is important to evaluate them to understand the performance and whether it is enough. This impetus for this work is to do just that with a focus on rural school buildings.

Residential buildings and cultural sites in the Kathmandu valley are predominantly constructed using unreinforced masonry as well (Chaulagain et al. 2016). Typical architectural designs of urban houses are characterized by Newari craftsmanship with wooden carved windows and

adobe tiles on the roofs (Figure 1 & Figure 2). A huge influx of domestic immigrants from rural places to Kathmandu and other major cities had increased the housing settlements in urban areas significantly in recent years. The built-up area in Kathmandu valley between 1992 and 2002 had an increase of 211 % and keeps increasing to date (NPC, 2015). Also, Reinforced Concrete (RC) construction started growing rapidly in urban areas since the 1980s.

2.2 Review of building specifications and code regulations

In 1994, the building codes for load-bearing URM were released: "Seismic Design of Buildings" (NBC 105:1994), "Masonry: unreinforced" (NBC 109, 1994), "Mandatory Rules of Thumb for Loadbearing Masonry" (NBC 202, 1994), and "Guidelines for Earthquake Resistant Construction: Low Strength Masonry" (NBC 203,1994), among others. The 1999 Building Act promoted safer building practices covering URM school buildings as well. URM can be regarded as synonymous with "non-engineered construction" practiced in rural Nepal where engineers were seldom available (NPC, 2015). Post-2015 improvements targeted the non-engineered construction with practical manuals, guidelines, on-site construction booklets, and mason training. In 2016, "Seismic Retrofitting Guidelines in Nepal" (CoRD, 2016) was published for adobe structures, masonry structures, and RCC structures covering both theoretical and practical aspects of seismic retrofitting, which has been pivotal in the reconstruction process as often is used by field engineers for the reconstruction of school buildings. It has fundamentally been used as a reference to train engineers and masons involved in the reconstruction overseen by the NRA (NPC, 2015). Additionally, design catalogs were released for template design drawings of earthquake-resilient buildings (DUDBC, 2015) and also for alternative building technologies (DUDBC, 2017).

There has been considerable improvement in the implementation of building guidelines overseen by government bodies post-2015 in Nepal. A federal system of governance was introduced in 2015, which can be seen as a positive change since resources can be allocated and used effectively at a local level (NPC, 2015). In the majority of municipalities, architects and engineers are required to submit a detailed (structural) design report for a building permit to be issued (DUDBC, 2018). However, consistent enforcement of standards and regulations varies at both provincial and central levels of government.

In the rural part of hilly regions in Nepal, natural stones are still abundantly available along the river banks (Pun, 2015). Sedimentary rocks have higher workability but wear out faster than other types of rocks; slate and marble are the most commonly used metamorphic building stones. The stone units are sometimes cut to brick-like pieces, and other times left as non-uniform stone. The NBC 203 (2015) code prescribes that the stones should be broken down not less than 50 mm in thickness and 150 mm in width and length before being laid, except in the case of through-stones. Through-stones extending the whole thickness of the wall should be used with the maximum horizontal spacing of 1200 mm and 600 mm in the vertical direction (Fig. 3). The irregular shape of stones usually creates a large space in between stones which should be filled with stones instead of only mortar. The mud mortar used should be free from any organic materials and pebbles that could hinder its desired applicability. The sand content in the mud shall not be more than 30 % to achieve proper cohesiveness.

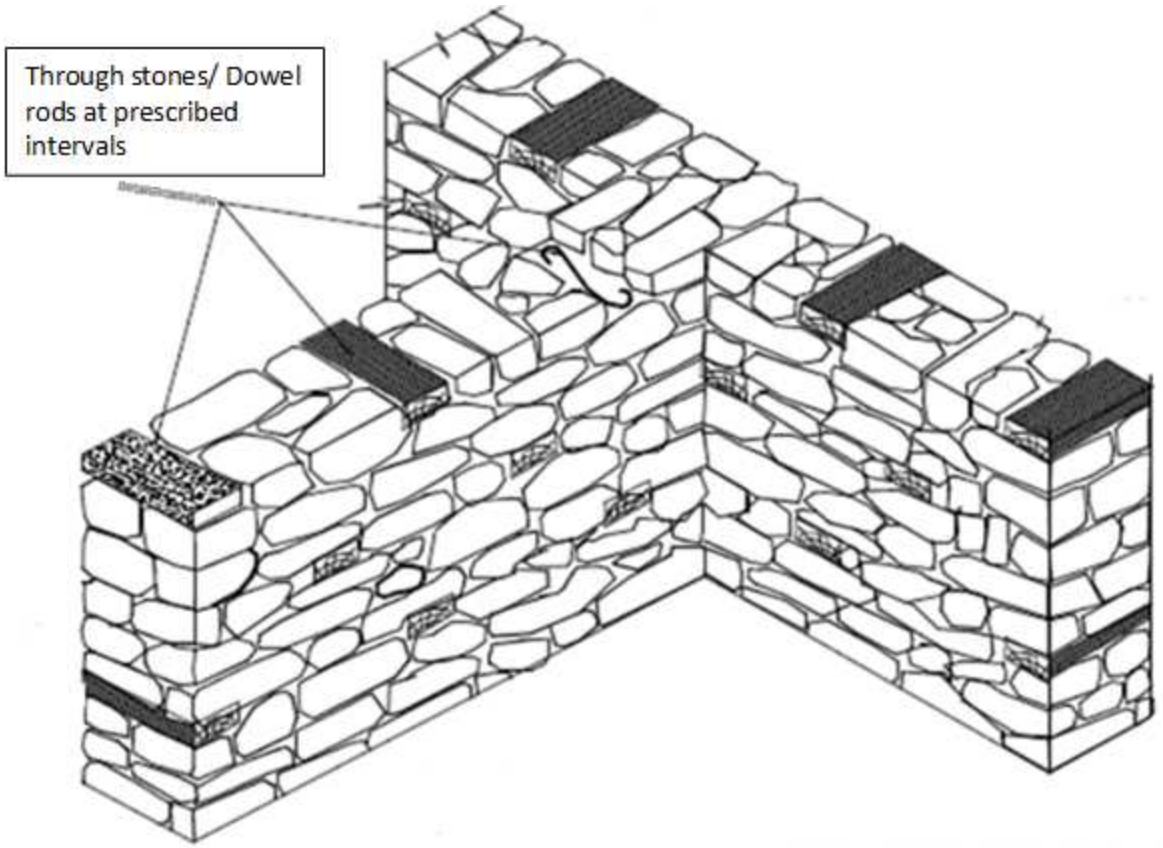

Fig. 3. Details of stone wall masonry construction (from NBC 203, 2015)

Also, according to NBC 203 (2015), the stone masonry buildings may have up to two stories and an additional attic floor. The wall thickness is typically prescribed to be from 35 cm to 45 cm for a single story, and 45 cm for a double story building. The maximum height (floor to floor) of a building shall not exceed 8 times the wall thickness at the superstructure. Mortar joints should be between 10 mm to 20 mm and the vertical joints should be staggered. For roof coverings, Corrugated Galvanized Iron (CGI) sheets are popular in most parts of the country, which are nailed to a wood roof frame of purlins and rafters for support (NBC 203, 2015).

As reported in the NPC (2015), most of the school buildings that suffered damage during the 2015 Gorkha earthquake were not compliant with any building codes or seismic provisions due to the historic lack of regulation and enforcement. The only building code practiced to some extent was the NBC 202 (1994) for Mandatory Rules of Thumb (MRT) specifications of reinforced concrete construction in urban areas (Chaulagain et al., 2016). Most tall structures or apartment buildings were designed according to the Indian Standard (IS) codes, which failed to address Nepal specific soil characteristics and seismic parameters leading to increased seismic vulnerability (Schildkamp et al., 2019)

The revised version of the seismic code, NBC 2015:2019, makes the code more effective in terms of acceptability, simplicity in application, and clarity in each clause, as presented in Maskey et al. (2020). The revised code has retained the probabilistic format of occurrence of the earthquake and incorporates two levels of earthquakes – earthquakes with return periods of 2,475 years and 475 years as the MCE and DBE. Also, in NBC 105:2020, the seismic hazard zoning map for Nepal in terms of peak ground acceleration (PGA) (as a fraction of gravity) for the return period of 475 years is presented and is referenced later in this thesis. Two response spectra developed based on the result of the probabilistic seismic hazard analysis; one for equivalent static method and another for the dynamic analysis, are incorporated in the code. Overall, the commentary to the NBC 105: 2020 facilitates in understanding the most recent clauses and rationale of the code provisions.

2.3 Damage assessment reports after 2015 Gorkha earthquake

Significant damage caused by the 2015 earthquake to URM buildings has led to efforts aimed towards reducing the vulnerability of this building type. CoRD (2016) describes some common failure types observed from post-earthquake damage assessments for building types ranging from, the vulnerability inherent to these building types, and analyzes possible retrofitting strategies.

CoRD (2016) classifies in-plane failure modes into diagonal shear cracks, vertical cracks, and cracks at corners. Due to flexible roofing and poor connections between walls and roofs, in-plane shear is relatively less common in URM-type buildings. The primary cause for collapse of buildings for unreinforced masonry in mud-mortar or adobe, is owed mainly to out-of-plane failure mechanisms (NPC, 2015). Any out-of-plane damage is a stability and equilibrium problem that falls under collapse damage criteria (Giordano et al., 2019). In buildings with weak wall-diaphragm action or weak wall-to-wall connection, the damage is governed by out-of-plane failure behavior including parapet and gable wall collapse/failure, delamination wall components (Penna et al., 2014).

This proportion was far less in the case of RC buildings, in which in-plane damage modes were predominant. RC buildings have been more widely studied, due to the emerging popularity of RC construction in recent times, particularly in urban and suburban areas. RC buildings are susceptible to damage types including soft-story failure, insufficient longitudinal reinforcement detailing, floating columns, concrete mixing, building asymmetry, load accumulation in upper stories, foundation problems, among other construction deficiencies (Gautam et al., 2016).

2.4 Experimental investigations on building materials and specifications

Understandably, the majority of school buildings lack effective provisions against seismic loading and are built to resist the vertical loads. However, many URM buildings, particularly in Nepal, are situated in high seismic regions are vulnerable to high seismic events. Therefore, significant lateral loads are also imposed on the building components. To obtain parametric values required for the seismic evaluation of these structures, static load tests and reduced or full-scale dynamic loading shake table tests are necessary and are reviewed in this section.

2.4.1 Static loading tests on stone or mortar units and wall specimens

The experiment conducted by Senthivel et al. (2009) on stone rubble masonry with mortar aligns with the housing typology for the URM in Nepal's context (Fig. 4). At a lower pre-compression level (100 kN), a progressive flexural failure mechanism was induced characterized by rocking or out-of-plane failure. Flexural cracking in the bed joints occurred when the tensile stress on a horizontal mortar joint exceeded the sum of the bond strength of that mortar joint and the frictional stress between the mortar and the units. An increase of axial stress, from 100 kN to 250 kN, caused a change in failure mode from flexure or rocking failures to shear rupture in the mortar interface. A diagonal shear failure occurred when the diagonal tensile stress resulting from the compression shear state exceeded the splitting tensile strength of masonry.

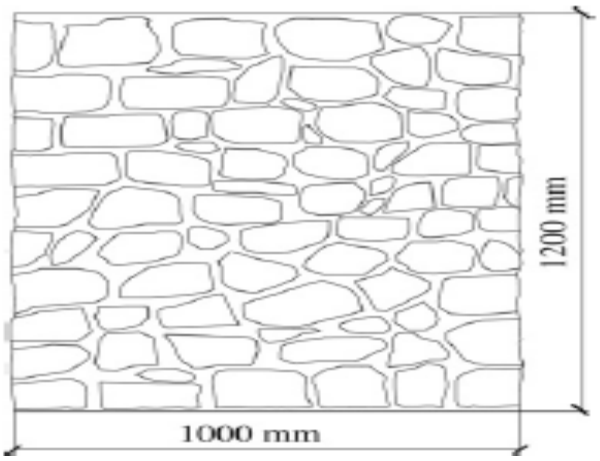

Fig. 4. Stone Rubble Masonry with mortar (From Senthivel et al., 2009)

In a static loading test conducted by Binda et al. (2006) to determine the properties of limestone and lime mortar, the compressive strength of the stone units was determined using three cylindrical specimens of 80 mm diameter and 145 mm height. The modulus of elasticity, compressive strength, and Poison's ratio of limestone was observed as 9.5 GPa, 20.6 MPa, and 0.10 respectively. The tensile strength of the stone was determined using a splitting test on six cylinders of diameter and a height of 80 mm sawn along the direction of bedding. The splitting tensile strength of limestone was 2.05 MPa. The flexural strength of lime mortar was determined using 40 mm x 40 mm x 160 mm prisms. The average value of flexural strength and compressive strength of lime mortar at 28 days was 1.5 MPa and 7.4 MPa, respectively.

Similarly, some other related experiments can be found in Vasconcelos G. (2005), in which the stone units, mortar cubes, and wall specimen were tested under compression, tension, and shear respectively. The average modulus of elasticity and compressive strength of stone was 20.2 GPa, 69.2 N/mm^2; while the tensile strength of mortar was 2.8 N/mm^2. In a static experiment by Build Change (2019), the average compressive strength of eight stone samples taken as representative samples from central and northern provinces of Nepal was found to be 30.4 MPa (CoV = 68%).

Similarly, the experimental tests by Pun (2015) reported the average compressive strength of stone units and mud mortar to be 37.91 MPa and 1.56 MPa, respectively.

Silveira et al. (2012) conducted extensive studies on the available data on the adobe constructions to compare with the properties of specimens extracted from ancient adobe buildings. Cylindrical specimens were extracted diameters of 80 to 90 mm and height approximately twice the diameter tested in compression and splitting. It was reported that the mean compressive strength, modulus of elasticity, and tensile strength of the adobe were 1.32 MPa, 225 MPa, and 0.17 MPa respectively. The differences in stone properties across these experiments demonstrate the importance of choosing a reliable data source that is closest to suit Nepal's building conditions.

Petracca (2015) makes use of an experimental test by Raijmakers and Vermeltfoort (1992) performed on shear walls made out of brick and mortar to observe the shear failure mechanisms conducted tests on masonry shear walls considering two wall types: i) with an opening in the center, hereby designated by "hollow wall," or a complete panel, hereby designated by "solid wall." The specimen consists of a pier with a width/height ratio of one (990 X 1000 mm^2), built up with 18 courses (16 active courses and 2 courses clamped in steel beams) of Joosten solid clay bricks (dimensions 204 X 98 X 50 mm^3) and 10 mm thick mortar (1:2:9, cement: lime: sand by volume). The piers were subjected to a vertical uniformly distributed load 0.3 N/mm^2 before a horizontal load was monotonically increased under top displacement control until failure. For the joints, the composite yield function described is adopted and, for the potential cracks in the bricks, a simple Mode I cracking model with exponential tensile softening and immediate drop to zero of the shear stress after initiation of the crack is assumed. The material data are obtained from the micro tension, compression, and shear tests are given before and are given in Table 1

Table 1. Inelastic Properties for Mortar Joints

Tension		Shear					Cap			
ft_o	G_t	C_o	tan Φo	tan Φ_r	tan Ψ_r	G_t	fm	C_{nn}	C_{ss}	C_n
0.25; 0.16; 0.016 N/mm^2	0.018 N/mm	1.4 N/mm^2	0.75	0.75	0	0.125; 0.05; 0.05 N/mm	10.5; 11.5; 11.5 N/mm^2	1.0	9.0	0 N/mm^2

While URM buildings are very common in Nepal, so too are URM buildings integrating timber elements. In these cases, timbers (mainly *Sal wood*) are used as framing components in URM construction for roof trusses, wooden beams and lintel bands, buttresses, and also for flooring (CoRD, 2016). Sekhar and Rajput (1968) measured the mechanical properties of Salwood specifically, collected from 14 localities of India. They found the modulus of elasticity and modulus of rigidity to be 14,710 N/mm^2 and 101.5 N/mm^2 respectively.

2.4.2 Shake table tests of stone masonry type buildings built in mud-mortar

While static loading tests are indispensable to obtain material properties of building components, shake table tests using dynamic loading are needed to exhibit the full behavior of a URM school building. The damage modes that propagate at different intervals of dynamic loading can be observed through these tests to better understand the structural performance of the URM-type buildings. Betti et al. (2014) conducted a shake table test with an unreinforced masonry prototype with flexible diaphragms until collapse. The masonry walls were constructed with calcareous tuff stones and lime-cement mortar with weight ratios of the components of 10.5 (sand), 11 (lime) to 1 (cement). The prototype house was a 1:1.5-scaled two-story building (Figure 8), aimed at reproducing the typical ancient masonry buildings based in Central Italy. The plan layout is made of a single cell with outer dimensions of 3.5 m × 3 m, while the inter-

story heights measure approximately 2.2 m. The masonry walls have a constant thickness of 0.25 m and are composed of vertical faces without any transversal connection with flexible timber floors. Each floor was built using five wooden joists with a section of 0.10 m × 0.18 m and wooden boards with a thickness of about 20 mm nailed to the wooden beams. The tests were carried out through the application of a normalized natural seismic input scaled at increasing intensity. The reference input was from the Umbria-Marche earthquake of 26 September 1997 (Richter magnitude of 6.1, epicenter in Annifo-Colfiorito. The compressive strength of the masonry was in the range of 2.0 to 3.5 N/mm^2. The unit weight of the stone units was observed to be 1700 kg/m^3. The tensile strength for diagonal shear was in the range of 0.06-0.07 Mpa.

Fig. 5. Shake table test of stone masonry building in lime mortar test specimen (from Betti et al., 2015)

In terms of the similarity to the stone masonry construction to Nepal's context, the selection of material properties of stone and mortar was derived and adjusted from related research works of Petracca (2016) and Build Change (2019) and are tabulated in Chapter 3.

2.5 Experimental investigations on seismic provisions and retrofitting strategies

This section sheds light on some of the experimental works performed to test various inclusions to improve seismic resilience like lintel bands, vertical reinforcements, and through-stones. For instance, vertical reinforcements are prescribed to be used in masonry walls at corners or next to openings, to prevent shear cracking (CoRD, 2016). However, Schildkamp et al., (2019) questioned whether a relatively small number of steel rods will provide sufficient ductility in such thick walls; also claimed that a vertical disruption in the critical connections may weaken, rather than strengthen the walls. Either experimental tests or accurate analytical modeling including these changes would be important to better answer these concerns. Hence, some of the more relevant tests useful to evaluate effective retrofitting strategies are discussed further.

A shake table test for two identical URM wall specimens was carried out in Pun (2015). The experiment was performed on two systems, one unreinforced, another reinforced with Galvanized Steel Wire (GSW). GSW is often used in retaining walls in many highway structures across Nepal. The shake table specimen was representative of a half-scale model of a part of a single-story room. Ground motion recording of the 1940 El Centro Earthquake was selected as the representative seismic loading. The motive of the experiment was to get the mechanical properties of the specimens and also to check the effectiveness of the GSW reinforcement technique. Under very extreme shaking, the model buildings showed significant sliding and rocking of stones in the in-plane wall panels and induced lateral displacement. Using Galvanized Steel Wire (GSW), two reinforced wall specimens (1,400 mm x 350 mm x 400 mm) were also prepared and tested in the lateral span. As seen from the experiment results, the ultimate strength of the reinforced wall specimen was almost 2.4 times that of the unreinforced specimen.

Magenes et al. (2010) conducted a full-scale shake table experiment for stone masonry in cement mortar, to extract mechanical properties and test the effectiveness of improving the connection of the ridge beam to the wall using an external steel anchorage through full-scale shake table tests, as seen in Fig. 6. The model was built with URM walls of a nominal thickness of 32 cm, which had two wythes of undressed stones (not cut or rendered smooth) built one close to the other with some smaller stones and mortar filling the gaps in between. The floor structure was made of 12cm wide and 16cm high pinewood joists placed every 50 cm with 30 mm thick planks simply nailed on top. The roof structure included one 20 cm x 32 cm ridge beam, two-segmented 32 cm x 12cm rafter beams on top of the longitudinal walls, and 8 cm x 12 cm purlins every 50 cm forming the two pitches with 3cm thick planks. The mean values of modulus of elasticity, compressive strength (f_m), tensile Strength for diagonal shear (f_t), and Shear Modulus (G) was observed to be 2,550 Mpa, 3.28 Mpa, 0.137 Mpa, and 840 Mpa respectively. It was seen from the experiment that prevented out-of-plane mechanism including gable wall failure during the repetition of the test in which the building behavior was mainly governed by the in-plane wall response.

Fig. 6. Floor and roof details with details of wall connection (from Magenes et al. 2010)

Meguro et al. (2012) performed shaking table tests on 1:4 scaled stone masonry houses, both with and without retrofitting with polypropylene band meshes. The specimens were a single room, one-story house with a pitched wooden roof but without gable walls. The dimensions of both models were 950 mm x 950 mm x 720 mm with 100 mm thick walls. The wall was constructed using pieces of stone of size 40 mm to 60 mm placed side by side in rows and gaps filled with gravels of size up to 10 mm and cement-lime-sand mortar (1:7:19). The water-cement ratio of the mortar was chosen as 0.15. In the case of a non-retrofitted specimen, cracks were initiated at the top of openings and propagated towards the bottom of the wall. With an increased loading rate, cracks widened further. As a consequence, the connection between walls got separated leading to complete collapse for the non-retrofitted specimen. The nature of crack initiation and propagation in the case of the retrofitted specimen was almost similar to the non-

retrofitted case. However, PP-band mesh prevented the collapse of the structure even when the base displacement was more than four times greater than a non-retrofitted case (Fig. 7).

Fig. 7. Level of collapse seen in the non-retrofitted house (left) and pp-band retrofitted masonry specimens (right) (from Meguro et al., 2012).

2.6 Numerical investigations of Nepalese structures

The numerical analysis should suffice to exhibit all types of relevant damage mechanisms that a structure may experience during seismic events. Hence, the modeling approach and software must be capable of predicting both global and local failure modes ranging from linear-elastic deflections to plastic failure mechanisms, and localized damage. The lack of lateral force-resisting components in the URM walls makes them vulnerable to earthquake loads. The behavior is strongly characterized by weak mortar interfaces which can undergo significant physical or mechanical degradation with time (Senthivel and Lourenco, 2009).

An initial step in performance-based seismic analysis is to determine measurable limit states that correspond to specific levels of damage. In Chaulagain et al., (2016) investigated three limit states (moderate damage, extensive damage, and collapse) into their analytical study; the limit states were based on the maximum global drift or maximum inter-story drift. In CoRD (2016), a collapse prevention performance objective permits extensive cracking, and noticeable in-plane and out-of-plane offsets but drift must not exceed 1%. For a life safety performance objective, extensive cracking and noticeable in-plane offsets are permitted in both structural and non-structural elements. Out-of-plane offsets must be minor and drift cannot exceed 0.6%. Finally, for the immediate occupancy and operational performance objectives, only minor cracking of the veneer is allowed with no noticeable out-of-plane offset, and drift must not exceed 0.3%. The value of the engineering demand parameter (e.g., inter story drift) associated with each limit state and performance objective varies by building type.

Fragility functions are often developed with experimental or analytical outputs, adopting these same limit states. In Giordano et al. (2019), fragility functions were developed for out-of-plane failures of URM walls. Capacity Spectrum Method was implemented using the corresponding periods and equivalent damping coefficients for each damage state. Monte Carlo Simulation was performed by randomly generating 10,000 combinations of the input parameters for analysis including wall thickness, elastic modulus, specific weight, and other loads. The results of the analysis were shown to be consistently lower than the observational values.

In Adhikari & D'Ayala (2019), Applied Element Method (AEM) was used in which a triangular 3-D mesh was first created, and then random shaped units were generated by clustering the triangular applied elements through unit springs to represent the irregular arrangement of stone units. Experimental tests were performed to analyze the damage modes for different load

combinations. Numerical outputs from Extreme Loading for Structures (ELS) software were compared against experimental findings. In the analytical model, the construction details natched Nepalese context of URM construction with stone. For uniaxial loading, the analytical model predicted the vertical and inclined cracks in the wall that were also observed in the experimental results. For combined compressive and lateral loading, the AEM was able to process the results for in-plane behavior, but not for out-of-plane collapse. Also, the out-of-plane behavior cannot be shown in the modeling work due to instability of models and convergence issues as a result of flexible diaphragm action.

One of the most commonly used numerical tools for the analysis of masonry structures is the Finite Element Method (FEM). Lourenco 2002 suggested three modeling strategies: micro-modeling, simplified micro-modeling, and macro-modeling. Of these three, micro modeling is the most detailed; the stone units and mortar are represented by continuum element whereas unit-mortar interface is represented by discontinuum element. In simplified micro modeling expanded units are represented by continuum element whereas the behavior of mortar joint and unit-mortar interface are lumped as discontinuum element. The mortar and unit mortar interface is lumped into average properties and units are extended to keep the geometry unchanged, thus masonry is considered as an elastic block connected by a potential crack joint. It has lesser accuracy as compared to the micro-model since Poisson's effect is not included.

Macro-modeling regards masonry as an equivalent homogeneous continuum, without making any distinction between units and joints in the discrete model. It can lead to issues related to the identification of mechanical properties and the definition of constitutive phenomenological failure criteria (Petracca, 2016). It involves breaking the wall into piers and spandrels in which only piers are assumed to undergo damage. The mechanical properties required in the macro-

modeling approach are taken from the average properties of the overall masonry unit. Ghosh et al. (1994) concluded that macro-modeling could predict the deformations satisfactorily at low-stress levels and inadequately at higher stress levels when extensive stress redistribution occurs. Pande et al. (1990) stated that macro-modeling would not accurately predict the stress distribution as the mortar interface is not separately modeled as in micro-modeling.

As highlighted in Petracca (2016), out-of-plane failure is caused when the deformation approaches the thickness of a wall instead of exceeding its bending strength. According to the paper, the 3D constitutive equations for thin shells or materials other than shells do not integrate the damage caused by transverse shear in the out-of-plane (thickness) direction. Therefore, accurate constitutive models are required to numerically reproduce the out-of-plane behavior of masonry. A new homogenization procedure for shell-like structures was proposed for micro-structures that are heterogeneous in the in-plane directions, but homogeneous in the thickness direction. Petracca (2015) further proposes an extension of fracture energy-based regularization to two-scale computational homogenization based on classical first-order continuum theory. Moreover, it is pointed out that in a FEM framework, the concept of strain-softening should not be considered as a characteristic of the material alone since it is related to both the fracture energy (Gf) and the size of the finite element where the energy dissipation occurs. The proposed model showed its capability at the micro-scale to represent the local tensile, compressive, and shear failures due to the complex interaction between units and joints.

Apart from analytical investigations to validate modeling approaches, such modeling can also be applied to test the effectiveness of seismic resilience features. In Bothara et al., (2018), the study was based primarily on experimental modeling, and numerical modeling was used only as a verification of the results of the shake table tests. The nonlinear finite element models for

unreinforced and semi-reinforced stone masonry walls were constructed using the finite element (FE) software TNO DIANA. Limitations in numerical modelings, such as the lack of continuum, variability in boundary conditions, material properties, and openings, were not addressed by the FE modeling approach used. Notably, the buttresses were able to prevent out-of-plane failure, thereby increasing the building's seismic capacity by more than 50% when compared to a building without buttresses and minimal reinforcement reduced the deformability of the building by almost three times.

Betti et al. (2015) simulated a wall to floor connection using a macro-element approach through the implementation of a non-linear algorithm in MATLAB. The macro-element approach was capable of predicting the collapse load but did not provide a satisfactory representation of the actual collapse mechanism. Notably, the applied hypothesis of rigid floors in the study does not work due to lack of floor connection to the adjacent walls and also due to the type of flooring materials used in Nepal's context (CoRD, 2016).

Senthivel and Lourenço (2009) carried out two-dimensional nonlinear finite element analysis to model deformation characteristics of historical stone masonry shear walls subjected to combined axial compression and lateral shear loading. A micro modeling technique based on plasticity theory was used for analysis. A good agreement was established through this process for the results derived from the experimental works of Vasconcelos G. (2009). The meshing was capable of exhibiting the mortar joints as planes of weakness and capable of capturing failure within the stone units. The finite element mesh was generated using a FORTRAN program. The units were modeled using eight-node quadrilateral iso-parametric continuum plane stress elements with quadratic interpolation and full Gauss integration. The mortar joints were modeled using a six node and zero thickness line interface elements with Lobatto integration.

In detailed micro-modeling, the stone units and mortar are represented by continuum element whereas unit-mortar interface is represented by discontinuum element. For mechanical properties, modulus of elasticity, Poisson's ratio and inelastic properties of both unit and mortar are considered and mortar interface is assumed as the plane of failure, thus enables the combined effects of units and mortar. In macro modeling the units, mortars and unit-mortar interface are considered as homogeneous continuum element. It does not consider the individual behaviour of unit and interface and treats the masonry as homogeneous anisotropic continuum element. It is simple and easy, be applicable where compromises between accuracy and efficiency is needed.

Given the findings based on this extensive literature review, the detailed micro-modeling approach is adopted here for analytical investigation. Many of the experimental studies are used for material properties and/or comparing analytical results. Details on the modeling approach are discussed in the next chapter of this thesis.

3 Methodology

3.1 Introduction to the numerical model used in the analysis

Advanced numerical methods are established as effective tools to understand and predict the behavior of masonry up to their complete failure, allowing to estimate the residual strength and safety of structures. The method used here is derived from Petracca et. al (2016) for the analysis of shells whose micro-structure is heterogeneous in the in-plane directions, but initially homogeneous in the shell-thickness direction, suitable for stone masonry wall typology. In this approach, the complete micro-structure (or a simplified version of it) is directly modeled, thus the complex interaction between the masonry constituents is naturally considered.

A 3-D constitutive model is adopted instead of a plane-stress one, to account for the transverse shear strain across the thickness direction (Petracca et. al, 2016). Due to the arrangement of the micro-structure, and the strong difference in mechanical properties of stone units and mortar, a significant amount of transverse shear appears in the (softer) mortar joints, in order to allow units to bend around the vertical axis of the wall. The numerical model of the specimen for the school building was carried out in Scientific Toolkit for OpenSees (STKO). The governing theories behind the workings of STKO application used for the micro-structural constituents are briefly presented here (see Petracca et. al, 2016 for more detail).

To begin with, the ultimate objective of this dynamic analysis is to solve the widely known equation of motion:

$$[M]\{\ddot{\mu}\} + [C]\{\dot{\mu}\} + [K]\{\mu\} = -[M]\{\ddot{\mu}_g\} \quad [1]$$

where, [M], [C], [K], are mass, damping and stiffness matrices, {ü}, {u̇} and {u}, are acceleration, velocity and displacement responses respectively and {ü$_g$}, is input ground acceleration. The corresponding displacements at an element level are translated using equation of motion to obtain global displacements.

The generalized unknown vector in the local coordinate system of the shell is defined where $u_0 = [u_x \quad u_y]^T$ are the in-plane displacements, u_z is the out-of-plane displacement, and $\theta = [\theta_x \quad \theta_y]^T$ are the out-of-plane rotations about the local x and y axes respectively. According to the first order shear deformation theory of Reissner-Mindlin, the generalized strains of the shell are defined as:

$$\hat{\varepsilon} = [\, \varepsilon_0 \; \kappa \; \gamma_0]^T = [\; \varepsilon_{0,xx} \;\; \varepsilon_{0,yy} \;\; 2\varepsilon_{0,xy} \;\; \kappa_{xx} \;\; \kappa_{yy} \;\; 2\kappa_{xy} \;\; 2\varepsilon_{0,xx} \;\; 2\varepsilon_{0,yz} \,]^T \qquad [2]$$

where ε_0, k, and γ_0 are the in-plane stress tensor, the curvature due to bending actions, and the transverse shear strain, respectively. Using the constitutive response of the shell, generalized stresses are given as:

$$\hat{\sigma} = [\, N \; M \; Q]^T = [\; N_{xx} \;\; N_{yy} \;\; N_{xy} \;\; M_{xx} \;\; M_{yy} \;\; M_{xy} \;\; Q_{xz} \;\; Q_{yz} \,]^T \qquad [3]$$

Where N, M and Q respectively represent the membrane force vector, bending moment vector and transverse shear force vector, per unit length. The generalized stresses and the tangent constitutive matrix for the shell can be finally integrated through the thickness, defining ζ as the through-the-thickness coordinate, ranging from -H/2 to H/2 (H being thickness of the wall). The Newmark integration scheme, also known as average acceleration method is used with parameters, with gamma and beta parameters equal to 0.5 and 0.25, respectively.

In a wall typology such as stone masonry load bearing wall, the mortar joints are softer compared to the stone units. Also, the thickness of the wall is in a much higher deformation range than the in-plane thickness of the wall (10 mm). However, the thickness strain component, ε_{zz} is not given with standard shell kinematics (see Equation 1.). Past constitutive laws failed to address the non-linear response in the mortar interface for transverse shear (Petracca et al., 2016). The kinematics of 3D layered shell formulation in STKO, however, can address the out-of-plane strain component, ε_{zz} is assumed constant in the thickness direction, and is calculated locally at each gauss point of the shell element.

3.2 Selected case building and specifications

The initial procedure involved creating a Representative Volume Element (RVE) using micro-modeling (Fig. 8.), representing coursed rubble masonry as units and 10 mm mud mortar as binders. The RVE is repeated throughout the wall topology to depict the random periodic nature of the stone and mortar configuration.

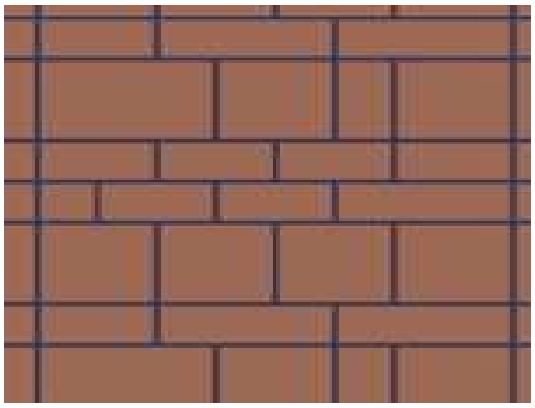

Fig. 8. Representative Volume Element (RVE) used in STKO model.

The material parameters governing the compressive behavior of mortar joints have been adapted to obtain the correct compressive behavior of the masonry composite material. The mortar spans throughout the whole thickness of the masonry wall in the horizontal direction. The properties of the stone and mortar are derived from Petracca (2016) and Build Change (2019), and are provided in Table 2; these properties are based on Continuum Damage Mechanics as briefly described in section 3.1.

Table 2. Elastic and inelastic material properties of stone and mortar joints

Material Properties	**Stone**	**Mortar joints**	**Units**
Modulus of elasticity, E	9,470	800	N/mm^2
Poisson's Ratio, ν	0.15	0.15	–
Tensile Strength, σt	2.05	0.25	N/mm^2
Tensile fracture energy, Gt	0.06	0.016	N/mm
Compressive elastic limit, σ0	20.6	2	N/mm^2
Compressive peak stress, σp	25	8.5	N/mm^2
Compressive residual stress, σr	4.4	2	N/mm^2
Compressive fracture energy, Gc	40	80	N/mm
Compressive strain at peak strength, εp	0.004	0.04	–
kb	1.2	1.6	–
k1	0	0.16	–

The building specimen, shown in Fig 9a., has walls constructed with masonry in mud mortar with a wall thickness of 35 cm and a building height of 2 m. The height of the gable wall is extended 0.6 m further to support the roof trusses, for transverse walls. As seen from the plan view drawing in Fig. 9b, the floor plan of the school building is 12 m x 4 m with 3 classrooms, and a wall thickness of 350 mm. The 3D layered shell element is able to capture the

heterogeneous property of the stone masonry wall across the thickness of the wall derived from shell kinematics (Petracca, 2016). The walls are assigned a face mass of 7.85E-07 N-s^2/mm^4, assuming that the mass density of the stone masonry walls is 22 kN/m^3. A 120 mm width global mesh is applied as quad topology (4-noded) for the shell element. The roof system is modeled using linear elements and the roof self weight is taken as 0.004 N-s^2/mm^3, assuming that the mass density (for Salwood roof truss) is 7 kN/m^3. In the roof and wall interface, macro-element with equivalent material properties for a composite stone and mortar masonry wall is used, for easy convergence in the boundary region between wall and roof. A new thin shell element was assigned for this portion of the model including a non-structured tria-topology for meshing in the region.

The base of the school building is constrained by single point constraints in both translation and rotation; while wall-to-wall and wall-to-roof interactions use multi-point constraints. Tzamtzis and Asteris (2004) did dynamic analysis of low-rise masonry wall by using quite high damping coefficients and found that the numerical simulation was matching with experimental results. For the problem under consideration, damping is applied using Rayleigh coefficients in wall elements using coefficients α and β taken as 0.05549 and 0.0105 respectively, for an initial damping of 6% and maximum value 10% considering stone masonry constructions as highly deformable, as derived from Tzamtzis and Asteris (2002). There are 30,250 nodes, 77,173 elements, 44,939 edges, and 31,418 faces obtained in the model after the final meshing was performed before running the Incremental Dynamic Analysis.

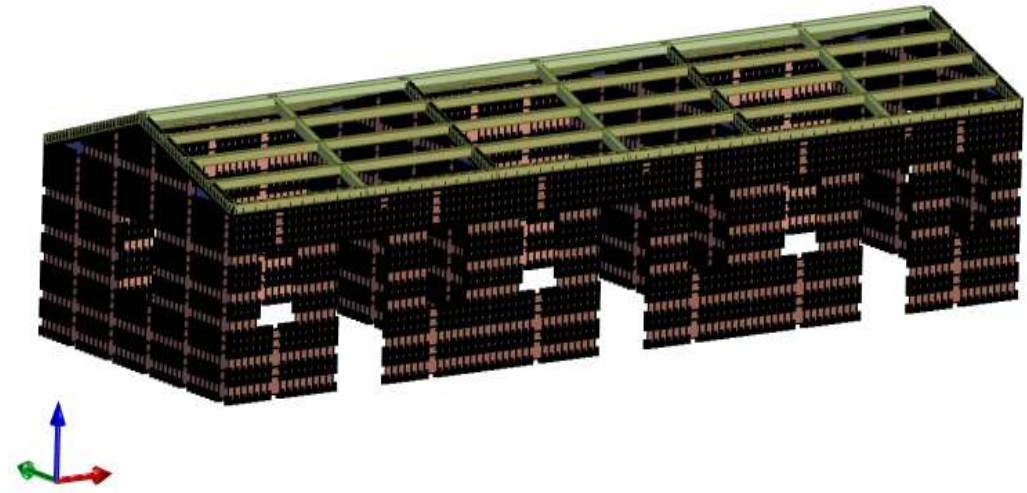

(a)

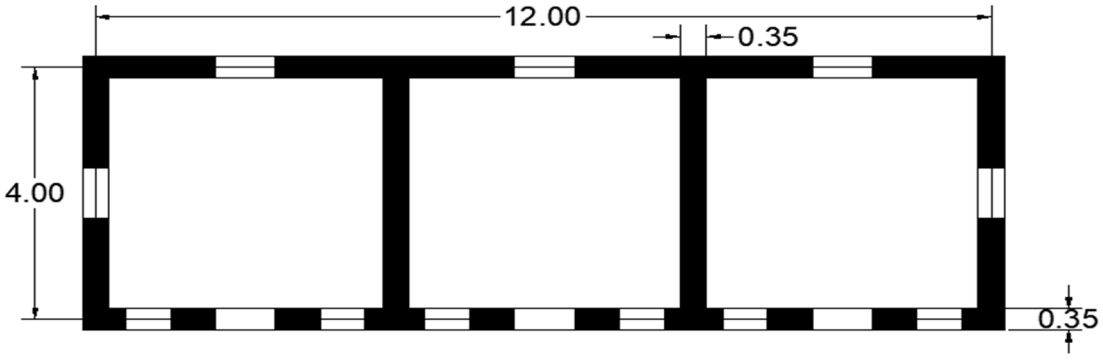

(b)

Fig. 9. Representative 3-D STKO numerical model for a single-story school building: (a) elevation view; (b) plan view

3.3 Selection of seismic sources and ground motions

Nonlinear response-history analyses (NLRHA) of the idealized 3D STKO model is performed for 7 ground acceleration records. Appropriate ground motions are selected from events having

magnitudes, fault distance, and source mechanisms that are consistent with the representative seismic parameters at majority of locations across Nepal. The only Nepali earthquake ground motion available is the 2015 Gorkha earthquake. To expand the analysis, appropriate simulated ground motions are used to make up for a total of seven ground motions.

The Main Himalayan Thrust (MHT) is identified as the major fault system running east-west across Nepal, and producing the largest earthquakes. It is a large, shallow-dipping reverse fault and surfaces at the Main Frontal thrust (MFT), accommodating roughly 20 mm/yr of shortening, along fault scarps from large past earthquakes have been found (Stevens et al., 2018). Besides MHT, other active source faults are the Eastern Nepal, Western Nepal and the Karakoram fault systems which fall under strike-slip faults. The search criterion to extract ground motion records considered these fault characteristics to generate corresponding strong motion records were derived from Stevens et al. (2018). The initial 100 records are based on disaggregated results of two prominent fault systems using $5<Mw<9$ and $20<Rrup<50$. The final selection of 7 records is based on the geographical proximity of other countries from Nepal and Vs30 (m/sec). The details of the seven selected acceleration records are provided in Table 3.

Table 3. List of ground motion records to be used as representative records for current seismic evaluation.

Earthquake Name	Year	Station Name	Magnitude	Mechanism	Rjb (km)	Rrup (km)
"Kobe_ Japan"	1995	"Kakogawa"	6.9	strike slip	22.5	22.5
"Kocaeli_ Turkey"	1999	"Iznik"	7.51	strike slip	30.73	30.73
"Manjil_ Iran"	1990	"Qazvin"	7.37	strike slip	49.97	49.97
"Chi-Chi_ Taiwan"	1999	"CHY035"	6.2	Reverse oblique	25.01	25.06
"Spitak, Armenia"	1988	"Gukasian"	6.67	Reverse oblique	23.99	23.99
"Tabas, Iran"	1992	"Bosrooyeh"	7.35	Reverse	24.07	28.79
“Gorkha_Nepal”	2015	Municipality Office, Kirtipur	7.8	Thrust	13	13

The selected ground motions consist of two horizontal components and a vertical component, each scaled to the target design spectrum for 5% damping and 500 yrs return period (Fig. 10.), is generated from SeismoMatch with the Importance Class set as “critical category” for school buildings; the highest seismic class of category and a zoning factor of 0.4g as suggested in past literatures (Gautam, 2018). SeismoMatch applies Spectral matching to scale the ground motions that involves modifying each frequency content of the time series record to match that of the design spectrum. The scaled processed records are obtained, which are subsequently used as increments to generate IDA and fragility curve for each limit states.

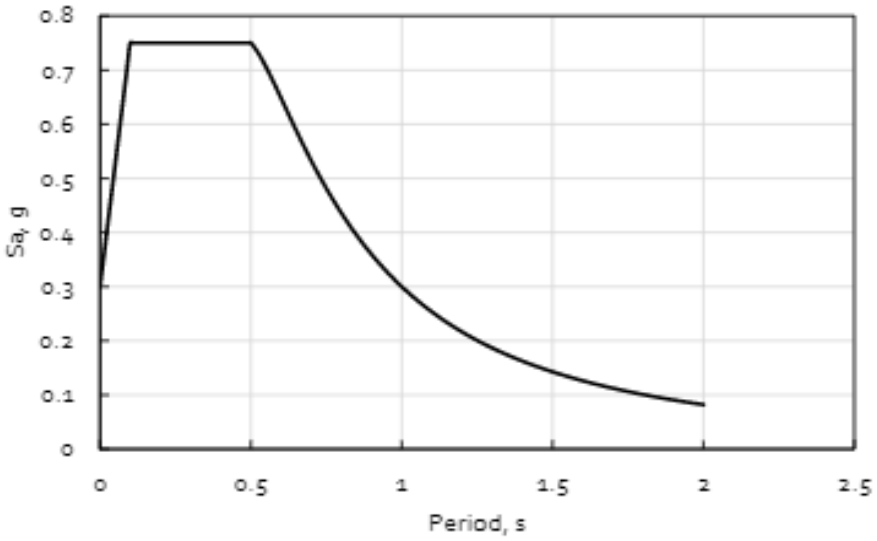

Fig. 10. Inelastic site spectrum as per NBC 2015: 2019

3.4 Proposed criteria for the definition of suitable limit states

Damage scale parameters are derived from NBC 105: 2020 for performance levels i.e. serviceability and ultimate limit state. Two structural limit states are adopted herein following requirements in the NBC 105 (2019). The first limit state, LS1, is the serviceability limit state set at not exceeding 0.6% inter-story drift (ISD). The serviceability limit state criterion requires the building to remain functional and must not cause occupants any inconvenience under usual conditions. The second limit state, LS2, is the collapse prevention (ultimate) limit state set at 2.5% ISD. These limit states ensure a reliable representation of the global building performance, considering the local damage evolution through micro-modeling parameters. The initial damage forms up at an element level within the mortar interface that subsequently shows a non-linear damage mechanism and translates to both in-plane and out-of-plane damage modes. At only

0.6% ISD, no structural damage should occur, and no more than hairline cracks will develop in the mortar. At 2.5% ISD, the structure is at risk of collapse due to in-plane or out-of-plane movement; structural and nonstructural damage will be present.

3.5 Nonlinear Dynamic Analysis Specifications

With more than 77,000 elements, and 63 analyses to perform (see next section for more details), analysis time was an important consideration. Analysis time depends on the duration and increment of the ground motion records. The average run time for a 25 seconds earthquake record takes over 8 hours for an average of 0.01 sec time increment in STKO on the author's computer. According to the IMPLEX method, proposed in STKO, the model did always converge in 2 to 3 iterations. To speed up the analysis, a timestep of 0.1s is selected; and recorded at a single step for every ten-time steps.

Additionally, other methods are used to generate more efficient computation such as increasing the mesh size in the global seed or reducing the number of fibers along the thickness (however, at least five are required)., without compromising the accuracy of final results. While performing the transient analysis using nonlinear parameters in STKO, Penalty method is used as a constraint handler as it is suitable to handle complex multi-point interactions between elements. Also, the Norm Displacement Increment Test is used for the convergence test because it converges the most easily for the constraint handler selected.

In post-processing the results in STKO, Petracca et. al (2016) makes use of a bi-dissipative d^+ / d^- damage model and defines the stress tensor as

$$\sigma = (1 - d^+)\,\bar{\sigma}^+ + (1 - d^-)\,\bar{\sigma}^- \qquad [4]$$

with $\bar{\sigma}^+$ and $\bar{\sigma}^-$ being respectively the positive and negative parts of the effective (elastic) stress tensor. d^+ and d^- are the tensile and compressive damage indexes, acting respectively on $\bar{\sigma}^+$ and $\bar{\sigma}$. The damage indexes are scalar variables ranging from 0 (intact material) to 1 (completely damaged material).

In order to identify "loading", "unloading" or "reloading" conditions of a general state of stress, two scalar measures are introduced, termed as equivalent stresses, τ^+ (tensile) and τ^- (compressive). The compressive surface and tensile surface can be considered to be evolving only if at least one principal stress is negative and positive respectively. These conditions are achieved through the Heaviside function, H(x) introduced in the following equation.

$$\tau^- = H(-\bar{\sigma}_{min})\left[\frac{1}{1-\alpha}\left(\alpha\bar{I}_1 + \sqrt{3\bar{J}_2} + \kappa_1\beta(\bar{\sigma}_{max}) + \gamma(-\bar{\sigma}_{max})\right)\right]$$

$$\tau^+ = H(\bar{\sigma}_{max})\left[\frac{1}{1-\alpha}\left(\alpha\bar{I}_1 + \sqrt{3\bar{J}_2} + \beta(\bar{\sigma}_{max})\frac{f_t}{f_{cp}}\right)\right] \quad [5]$$

where,

$$\alpha = \frac{\kappa_b - 1}{2\kappa_b - 1}; \beta = \frac{f_{cp}}{f_t}(1-\alpha) - (1+\alpha) \quad [6]$$

where $\bar{I}_1$ is the first invariant of the effective stress tensor, $\bar{J}_1$ is the second invariant of the effective deviatoric stress tensor, $\bar{\sigma}_{max}$ is the maximum effective principal stress f_t and f_{c0} are elastic limits in uniaxial tension and compression; f_{cp} is the compressive peak stress, k_b is the ratio of bi-axial to uniaxial compressive strengths, and the term f_t/f_{cp}. The constant k_1 controls shear behavior of the model acting on the shape of the compressive surface. Other two scalar

quantities, termed as damage thresholds $r^{\pm}$, are introduced to represent the largest values attained by the equivalent stresses $\tau^{\pm}$.

$$r^{\pm} = \max\left(r_0^{\pm}, \max_{0 \le n \le t} \tau_n^{\pm}\right), \; r_0^{+} = f_t, \quad r_0^{-} = f_{c0} \qquad [7]$$

where $r_0^{\pm}$ represent the initial tensile and compressive damage thresholds (i.e. the elastic limits in uniaxial tension f_t and compression f_{c0}, and n denotes the time instant.

3.6 IDA and Fragility curve development

Incremental dynamic analysis (IDA) (Vamvatsikos and Cornell 2002) is an efficient and rigorous tool for seismic demand analysis, specifically in the probabilistic domain. An IDA consists of a series of nonlinear response history analyses (NLRHA) performed on a structure using a range of scaled ground acceleration records. The basic objective of an IDA is to cover the whole range of response from the linear elastic to the nonlinear behavior, and finally to the collapse/instability of the structure. The IDA performed in this study extracts multiple curves for a suite of time history records, with damage parameter being the peak drift ratio.

The IDA is performed here by scaling the east-west, north-south, and vertical components of ground motion records (GM-01 to GM-21) to a desired PGA. The number of times the records are scaled should be based on the expected performance of the structure being investigated. For example, to capture linear elastic behavior, ground motion records are scaled to have low PGA values, e.g., near zero or 0.1g. To capture instability and collapse, ground motions should be

scaled to have high PGA values, such as 2.0g. Small increments between these two extents are necessary to understand differences in behavior occurring between no damage and collapse. Here, the ground motions are scaled from 0.1 to 1.3g using multiple increments along both building axes resulting in 63 total simulations. From the IDA data, the probability of failure can be calculated at each IM level by counting the number of IDA curves that cross the vertical line corresponding to the limit state under consideration. The ratio of these IDA curves to the total number of IDA curves (49 in this case) is the probability of failure at that level of IM, which is also the fragility. Given the available and selected information, these are the 'actual' fragility values based on the IDA. Fragility functions may also be derived from the data, expressed as

$$F(x) = P[X \leq x \mid PGA = g] \quad [8]$$

Where X is the maximum inter-story drift from each of the 49 analyses, x is 0.6% or 2.5% ISD for LS1 and LS2, respectively, for the given Peak Ground Acceleration (PGA) of the corresponding NLRHA. Eq. (8) is plotted using a cumulative distribution function of X using a lognormal distribution.

4 Results and Discussion

This chapter presents the results of the NLRHA in detail, based on specific limit states and corresponding intensity measures. A modal analysis is conducted to verify the time period of the single-story school building. According to the modal analysis conducted in STKO, the first mode of vibration is translation across the x-direction with a time period (T_1) of 0.1 seconds, which compares well with the relation prescribed in NBC 2015 (2019) for low strength stone masonry buildings. Also, it can be seen later in the section that the fragility values compare well with similar seismic evaluation conducted by Adhikari et al. (2019) for a double-storied Nepali stone masonry building.

4.1 Limit states and Failure modes

The overall global failure mechanism can be verified from similar analytical studies by Adhikari et al. (2019) and empirical observations after the 2015 Gorkha earthquake by Gautam et al. (2018). Although, the limit states and analytical methods are different as compared to previous studies, the propagation of failure starting from gable walls and wall-corners to out-of-plane failure of wall units are observed to be comparable. Past approaches failed to include material nonlinearity especially in the mortar interface where transverse strain induces out-of-failure including delamination and gable wall toppling. The technique adopted here allows the inclusion of the transverse strain component to accurately represent failure across the out-of-plane direction.

As can be seen in Fig. 11., the serviceability limit is reached once horizontal and vertical cracks start forming along the gable walls in the short wall and at openings along the main wall, till the output deformation of 15.6 mm, or 0.6% in inter-story drift is reached. The seismic bands and the

confining elements around the openings somewhat contain and prevent the diagonal shear failure of masonry wall portions till the LS1 is reached. The damage modes are further verified from past empirical observations after the 2015 Gorkha earthquake (as shown in Gautam, 2018) which suggests low to moderate damage scales including hairline cracks in gable walls for similar damage states.

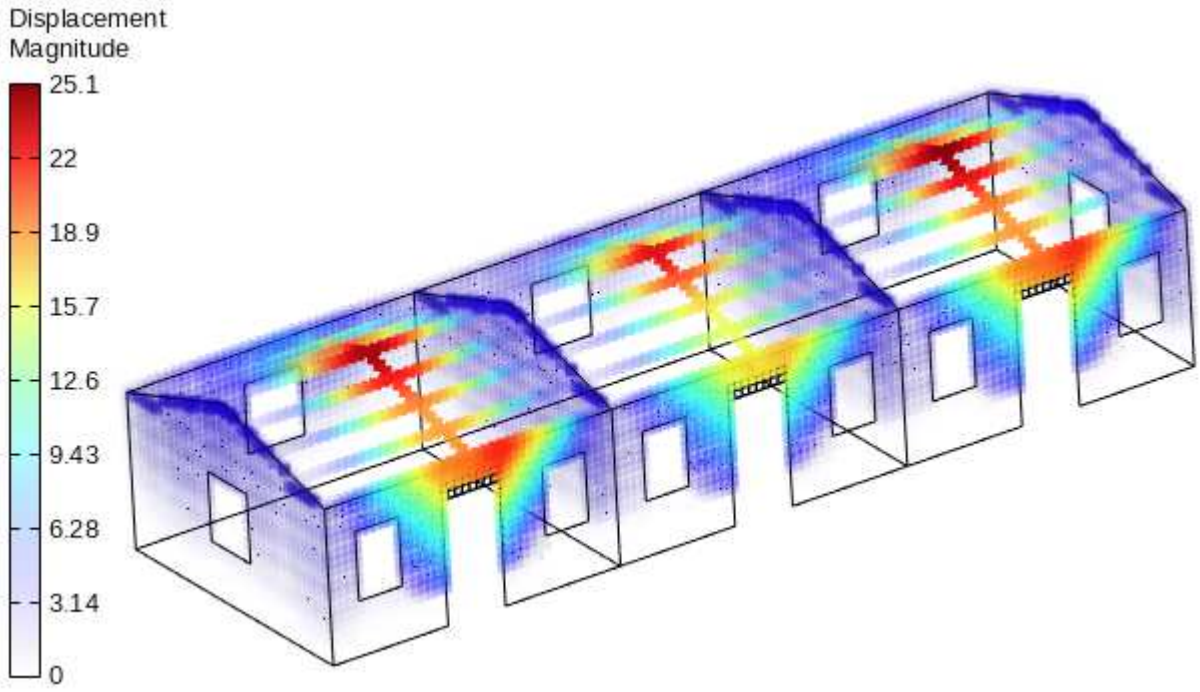

Fig. 11. Serviceability limit states: Maximum crack opening at about 15.6 mm. Hairline cracks appear at corners of openings and gable wall.

The out-of-plane collapse is seen to be dominant in the case of Nepali stone masonry buildings. Apart from out-of-plane collapse, heavy gable collapse is another common damage mode in affected single-story school buildings. It is caused by shear sliding failure of masonry portions at the wall-band horizontal interfaces resulting in the compression failure at the corner and around

openings (see Fig. 12.). Such shear-sliding failure damage modes are typical when there is low vertical pre-compression and poor-quality mortar (Tomazevic, 1999). LS2 is reached when the out-of-plane deformation output is around 65 mm, and the visual output representation is as shown in Fig. 12.

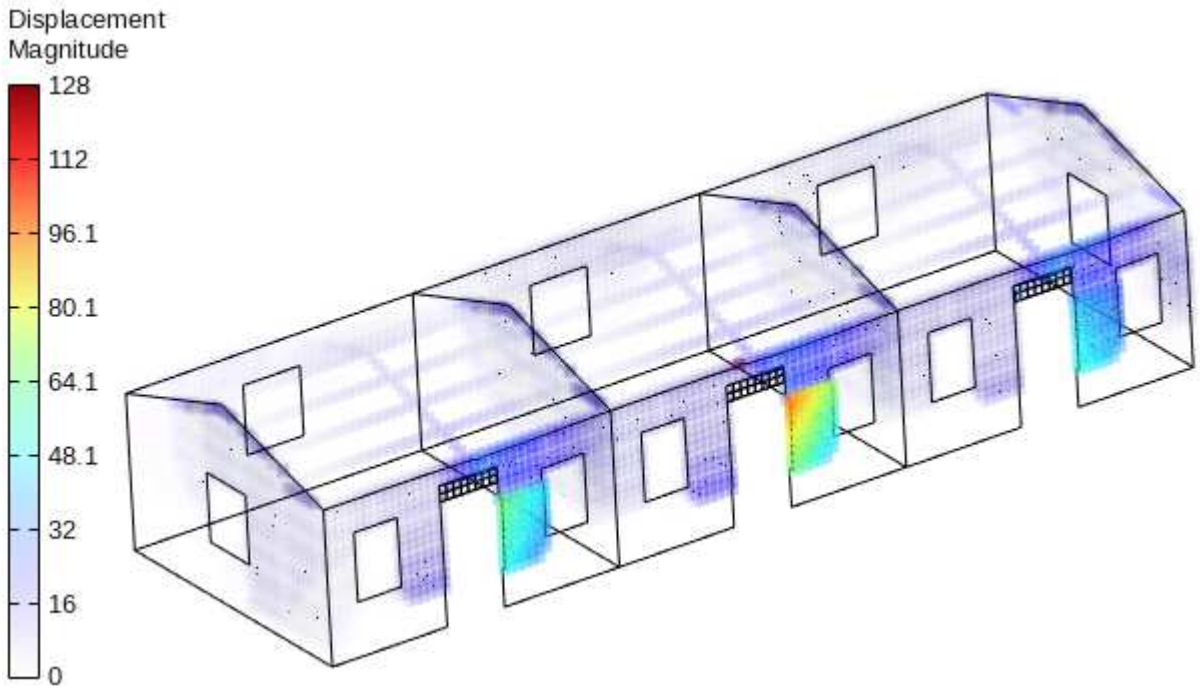

Fig. 12. Ultimate limit state: Maximum crack opening of around 65 mm. Widely distributed major cracks in all wall surfaces.

The overall building collapse is shown in the following Fig. 13, post the ultimate limit state. Mass irregularity, segregation of mud mortar and stone masonry units, diagonal shear cracks, tensile cracks, lack of connection between the orthogonal walls, delamination of stone and mortar units, and wedge-shaped failure at the corner were other noted damage modes in the collapsed buildings. The analysis successfully portrays all these failures with the micro-model capable of capturing all the intermediate damage states.

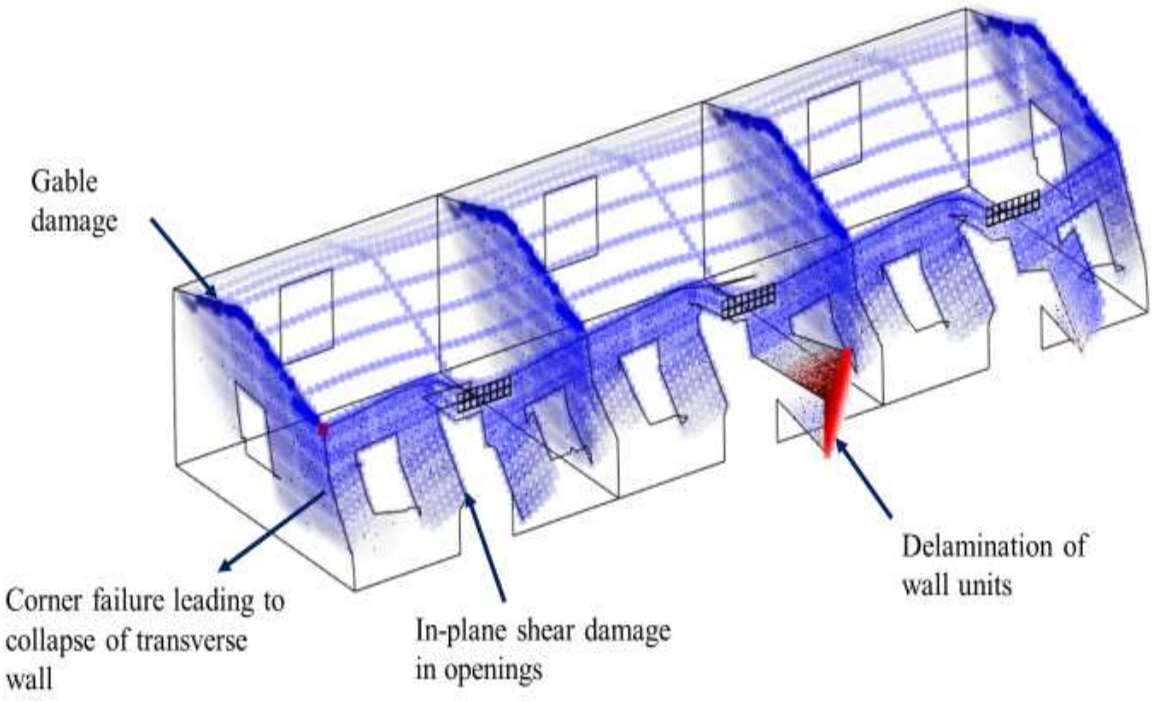

Fig. 13. Ultimate limit state: Maximum crack opening less than 65 mm. Widely distributed major cracks in all wall surfaces.

4.2 Incremental Dynamic Analysis (IDA) and Fragility Curves

The seismic capacity and failure mechanisms of the selected school building typology is assessed considering the uncertainty in ground motions through IDA. As there are limited ground motion records available in Nepal's context, a suite of seven records scaled to seven incremental peak

ground acceleration (PGA) values (0.1g, 0.3g, 0.4g, 0.55g, 0.7g, 1.0g, and 1.3g) are used to consider the record-to-record variability. The results of the NLRHA are obtained after running the complete suite of IDA records. To present the results of the IDA, the maximum drift, considering both x- and y- building axis, is taken and presented in Fig. 12a. The median response from the 7 records is presented in Fig. 12b. Looking at Fig. 12a, LS1 (serviceability at 0.6% drift) was reached with PGA ranging from 0.40g to 0.53g, whereas LS2 (ultimate at 2.5% drift) was reached with PGA ranging from 0.52g to 0.6g.

The results are expressed in terms of the probability of not exceeding inter-story drifts for three specific PGA values, 0.4g, 0.55g, and 0.7g, in Fig. 14. Although the datasets were generated for seven records, increments lower than0.3g were too small to generate the first limit state and increments above 0.7g were certain to cause collapse and exceed the second limit state, as evident in Fig. 13. In that regard, the probability of non-exceedance of the limit states against inter-story drifts for specific PGA increments is included in the fragility curve, unlike previous approaches to plot probability of non-exceedance against Intensity Measure (IM) for each limit state.

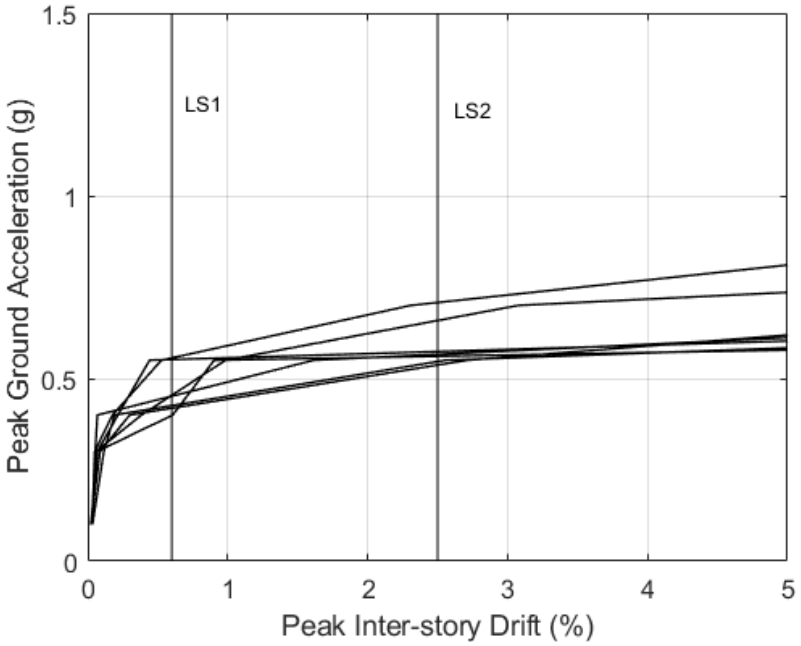

(a)

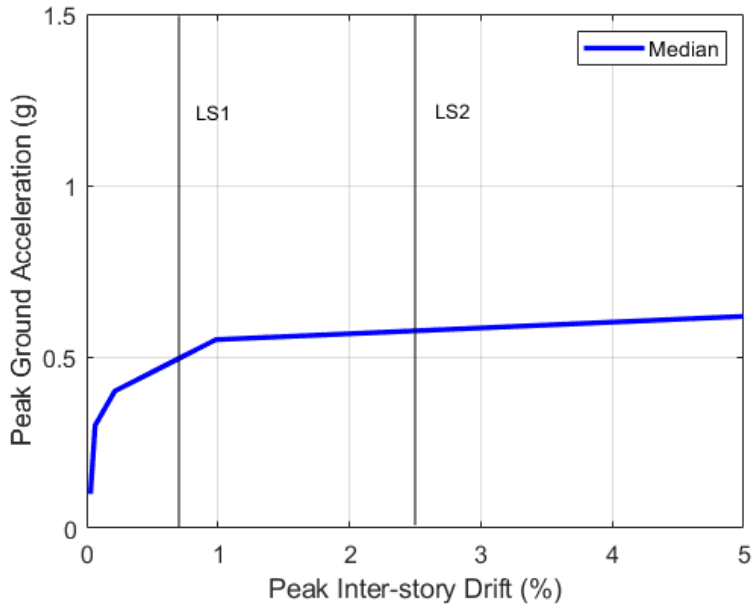

(b)

Fig. 14. IDA results: (a) 7 ground motions; (b) median response

A high degree of sensitivity of damage scales for lower interval of PGA is observed for the stone masonry building typology considered, which is highly brittle with non-linear deformation initializing as early as 0.3g for some records. The probability of non-exceedance for first limit

state is very high at 0.4g, with almost all the records failing to reach LS1= 0.6%. Comparatively, the probability of non-exceedance for PGA 0.55g at LS1 is 20% whereas for LS2, the probability of non-exceedance is approximately 90%, as seen from Fig. 15. The probability of non-exceedance for a PGA value of 0.7g pushes the building to ultimate limit state with about 95% certainty. Thus, it should be noted that, in the case of strong shaking, most of the stone masonry buildings in Nepal would be heavily damaged that could result in large number of fatalities.

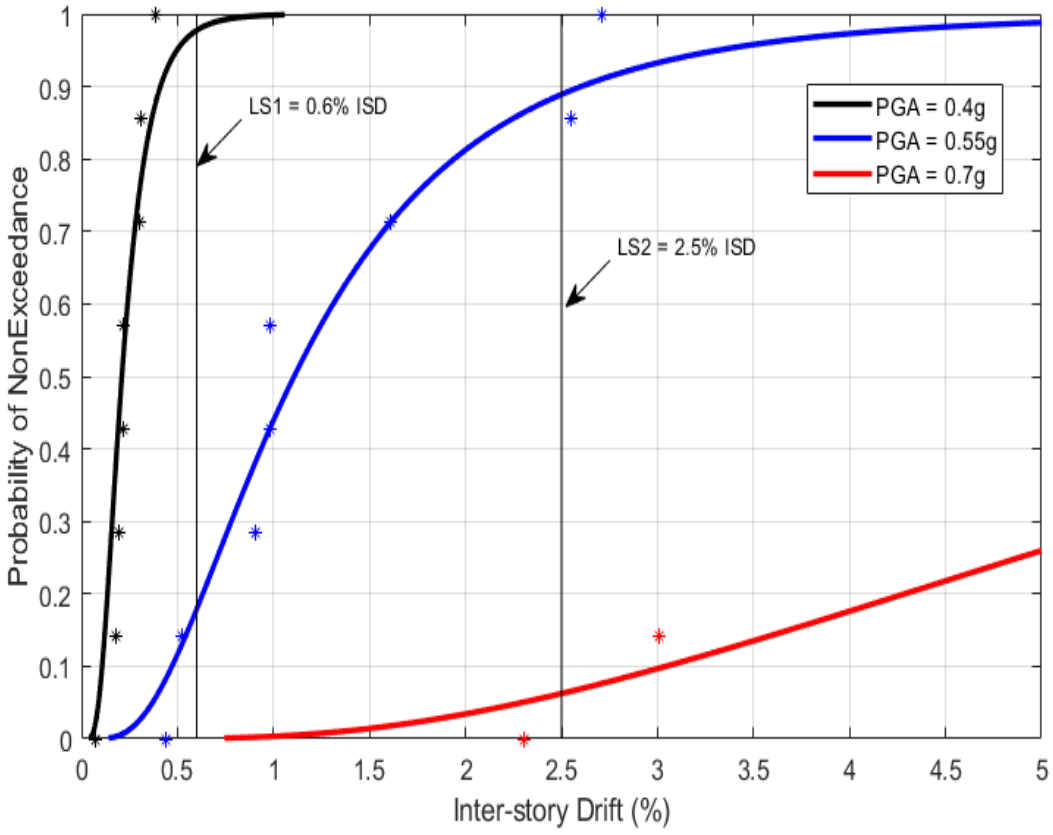

Fig. 15. Fragility function for rural Nepali school building generated from IDA

5 Conclusion

This thesis has proposed a computational homogenization method based on thick shell theory, to be able to provide equivalent response in terms of generalized strains and generalized stresses, from an iterative non-linear procedure. The method is designed to deal with micro-structures that is heterogenous in the in-plane direction, but homogeneous in the out-of-plane direction. Under this hypothesis, STKO allows to model the representative volume element (RVE) including its inherent constitutive laws and translate that damage to a global scale. The method has been applied to the analysis of a rural stone masonry school building in Nepal's context and similar building typology elsewhere.

In Adhikari et al. (2019), the median PGA for the first limit state of 0.6% inter-story drift was around 0.3g, whereas this thesis suggests that the median PGA is around 0.55g for LS1. Analyzing the novel micro model of the Nepali school building, it is observed that the performance of the building does improve slightly after including lintel bands and good roof-to-wall connection, as compared to past studies carried out by Adhikari et al. (2019) for buildings built before the 2015 earthquake. Further, the collapse mechanism for our model starts to show at a median PGA of 0.7g with 95% certainty. This does not provide confidence for occupants of these structures in Nepal when the next large earthquake occurs.

Seismic design practice in Nepal has noticeably improved after the 2015 earthquake sequence as seen from the discussion of construction characteristics of newly built post-earthquake houses. This thesis emphasizes further on the importance of providing lintel bands along the openings and addition of dowels connecting these to the walls to prevent vertical cracks along wall edges and to improve overall ductility. It is important for the tensile and compressive strength of mortar

to be increased to provide better resistance against shear damage failures. Vertical reinforcements are also recommended in the NBC 105 (2020), but not included in the STKO model. The gable wall system could be altered or strengthened with additional reinforcements to improve upon the initial damage propagation.

This study is one of the first attempts to formulate the fragility functions for the stone masonry buildings in Nepal using a novel micro-modeling approach. Although the adopted analytical approach proved to be successful in generating reliable fragility curves, some areas could still be improved for future research works. The results could have been made more comprehensive by adding another building model in the NLRHA, including one that did not include the lintel band, and a third model that incorporated a further seismic performance advancement beyond the lintel band. There is still large variability across different parts of Nepal in material variability and thereby material properties. Hence, the analysis could have been conducted for varying material properties from low to high quality to check their respective fragility. Running the IDA for additional PGA scales, particularly in the sensitive range of 0.4g to 0.7g and for more earthquake records could have yielded different results from what was presented in Figs. 12 and 13.

Future studies should target experimental investigations including shake table tests specific to Nepal's context. Since the proposed method involves heavy computation for multiple limit states-based fragility estimations, more ways could be investigated to simplify the computation. The modified method, while reducing computational costs to the level of the method practiced currently, provides better estimates of fragility at all limit states. This is shown through both quantitative and illustrative comparisons.

Overall, this thesis applied a novel micro-modeling approach to model a rural school building in Nepal. The school building modeled in this study provides several advancements compared to other available numerical studies, including (a) incorporation of a lintel band above all openings, following the changes in seismic provisions following the 2015 Gorkha earthquake intended to eliminate diagonal shear cracks in openings, (b) modeling supports to improve the roof to wall connection, and (c) modeling a realistic roof mass with credible material properties assigned on top of the wall system, where previous studies lumped the roof mass on top of the wall systems (see Parajuli, 2009). The seismic performance of the school building was characterized using Incremental Dynamic Analysis, and presented as a fragility function that can be used in seismic design and to inform future improvements to Nepal's seismic design provisions.

References

Adhikari, K.R. & D'Ayala, D. (2020). 2015 Nepal earthquake: seismic performance and post-earthquake reconstruction of stone in mud mortar masonry buildings, *Bulletin of Earthquake Engineering*.

Betti, M., Galano, L., & Vignoli, A. (2015). Time-History Seismic Analysis of Masonry Buildings: A Comparison between Two Non-Linear Modeling Approaches. *Buildings 5, no. 2: 597-621.*

Binda, L., Pina-Henriques, J., Anzani, A., Fontana, A. & Lourenço, P.B. (2006) A contribution for the understanding of load-transfer mechanisms in multi-leaf masonry walls: Testing and modeling, *Engineering Structures, vol. 28, no. 8, pp. 1132-48.*

Borst R (1991) The zero-normal-stress condition in plane-stress and shell elastoplasticity, Communications in applied numerical methods

Bothara, J., Ingham, J, & Dizhur, D. (2018). Understanding, experience and research on seismic safety of low-strength loadbearing masonry buildings, *16th Symposium on Earthquake Engineering, Roorkee, India.*

Bothara, J., Ingham, J, & Dizhur, D., Dhakal, P. R. (2018). The challenges of housing reconstruction after the April 2015 Gorkha, Nepal Earthquake.

B.S.J.B. Rana (1935), Great Earthquake of Nepal [Nepalko Mahabhukampa, in Nepali], Jorganesh Press, Kathmandu.

Build Change (2019), Laboratory Test Report Compression Test on Stone Masonry in Mud Mortar, Lalitpur, Nepal

CBS (2012). National Population and Housing Census 2011 (National Report), National Planning Commission Secretariat, Government of Nepal.

Chaulagain, H, Silva, V., Rodrigues, H., Spacone, E., Varum, H. (2014). Earthquake Loss estimation for the Kathmandu Valley*, Second European Conference on Earthquake Engineering and Seismology (2ECEES).*

CoRD (2016), Seismic Retrofitting Guidelines of Buildings in Nepal (adobe, masonry, RCC), Center of Resilient Development (CoRD) and MRB Associates, Department of Urban Development and Building Construction, Ministry of Urban Development, Government of Nepal.

Corradi, M., Borri, A., & Vignoli, A. (2003) Experimental study on the determination of the strength of masonry walls, *Construction and Building Materials.*

Department of Urban Development Building Construction (2018), Required Documents for Design Check (http://www.dudbc.gov.np/download/cat/)

DUDBC (2015), Design Catalogue for Reconstruction of Earthquake Resistant Houses, Vol. I. Department of Urban Development and Building Construction, Ministry of Urban Development, Government of Nepal.

DUDBC (2017), Catalogue for Alternative Construction Materials and Technologies, Department of Urban Development and Building Construction, Ministry of Urban Development, Government of Nepal.

Gautam, D. (2018) Observational Fragility Functions for Residential Stone Masonry Buildings in Nepal, *Bulletin of Earthquake Engineering 16, pages 4661–4673(2018).*

Gautam, D, Rodrigues, H., Bhetwal, K.K., Neupane, P., & Sanada, Y. (2016) Common structural and construction deficiencies of Nepalese buildings, *Innov. Infrastruct. Solut. (2016) 1:1.*

Ghosh A.K., Amde A.M., Colville J. (1994) Finite element modelling of unreinforced masonry, *10th international brick/block masonry conference.*

Giordano, N., Luca, D. L., Sextos, A., Maskey, P.N. (2019) Derivation of fragility curves for URM school buildings in Nepal, *13th International Conference on Applications of Statistics and Probability in Civil Engineering (ICASP13), South Korea.*

Giordano, N., Luca, D. L., Sextos, A., Cortes R. F., Ferreira F. C., Wu J. (2020) Empirical seismic fragility models for Nepalese school buildings, *Natural Hazards: Journal of the International Society for the Prevention and Mitigation of Natural Hazards, 2021, vol. 105, issue 1, No 18, 339-362*

Guragain, R. & Dixit, A.M., Meguro, K. (2012) Development of Fragility Functions for Low Strength Masonry Buildings in Nepal using Applied Element Method, 15 WCEEE, Lisboa.

HRRP (2018) Housing Typologies: Earthquake Affected Districts, Housing Recovery and Reconstruction Platform (HRRP), Nepal.

Lyndon B. Johnson (LBJ) School of Public Affairs (2018) Post-Earthquake Home Reconstruction in the Surrounding Hills of Kathmandu Valley, Nepal, *Policy Research Project Report 200.*

Magenes, G., Penna, A. & Galasco, A. (2010) A full-scale shaking table test on a two-story stone masonry building, *Proceedings of the 14th European conference on earthquake engineering, pap. No. 1432, Ohrid.*

Mouyiannou, A., Rota, M., Penna, A., & Magenes, G. (2014) Identification of Suitable Limit States from Nonlinear Dynamic Analyses of Masonry Structures, *Journal of Earthquake Engineering 18(2):231-263.*

National Society for Earthquake Technology-Nepal (NSET-Nepal) (2000) Seismic vulnerability of the public-school buildings of Kathmandu valley and methods for reducing it, *A report on Kathmandu valley School Earthquake Safety Program (SES) of the Kathmandu Valley Earthquake Risk Management Project (KVERMP).*

NBC 105 (1994) Guidelines for Earthquake Resistant Building Construction: Low Strength Masonry, Department of Urban Development and Building Construction, Government of Nepal.

NBC 105 (2020) Seismic Design of Buildings in Nepal, Department of Urban Development and Building Construction, Government of Nepal.

NBC 109 (1994) Masonry: Unreinforced, Department of Urban Development and Building Construction, Government of Nepal.

NBC 202 (1994) Mandatory Rules of Thumb for Loadbearing Masonry, Department of Urban Development and Building Construction, Government of Nepal.

NBC 203 (1994) Guidelines for Earthquake Resistant Construction: Low Strength Masonry, Department of Urban Development and Building Construction, Government of Nepal.

NBC 203 (2015) Guidelines for Earthquake Resistant Building Construction: Low Strength Masonry, Department of Urban Development and Building Construction, Government of Nepal.

NPC (2015), Nepal Earthquake 2015: Post Disaster Need Assessment, Vol. B, National Planning Commission, Government of Nepal.

NPC (2018), Multidimensional Poverty Index: Analysis towards action, National Planning Commission, Government of Nepal.

Pande G.N., Liang J.X., Middleton J. (1990) Equivalent elastic moduli for brick masonry *Comput Geotech 1990;8:243-65*.

Parajuli, H.R. (2009). Dynamic analyses of low strength masonry houses based on site specific earthquake ground motions, PhD thesis, Kyoto University.

Penna, A. (2014) Seismic assessment of existing and strengthened stone-masonry buildings: critical issues and possible strategies, *Bull Earthquake Eng.*

Petracca, M. (2016). Computational Multiscale Analysis of Masonry Structures, PhD thesis, Technical University of Catalonia.

Pun, R. (2015). Improvement in seismic performance of stone masonry using galvanized steel wire, PhD Thesis, University of Technology.

Raijmakers T, Vermeltfoort A (1992) Deformation controlled tests in masonry shear walls: report B-92-1156.

Schildkamp, M. & Araki, Y. (2019) School buildings in rubble stone masonry with cement mortar in seismic areas: literature review of seismic codes, technical norms and practical manuals. *Front. Built Environ. 5:13.*

Schildkamp, M. & Araki, Y. (2019) Cost analysis of mountain schools in nepal: comparison of earthquake resistant features in rubble stone masonry vs. concrete block masonry. *Front. Built Environ. 5:55.*

Sekhar, A.C. and S.S. Rajput (1968) Physical and Mechanical Properties of Sal (Shorea Robusta) from fourteen different localities in India, *Timber Mechanics Branch, Forest Research Institute & Colleges, Dehra Dun.*

Shrestha H.L., Chapagain N., Dhital R.K., and Adhikari S. (2016) Geospatial Analysis of Forest Resources Availability for the Reconstruction after Earthquake 2015, *International Federation of Surveyors, Article of the month- February 2016*.

Silveira, D., Varum, H., Costa, A., Martins, T., Pereira, H. & Almeida, J. (2012) Mechanical properties of adobe bricks in ancient constructions, *Construction and Building Materials, vol. 28, no. 1, pp. 36-44.*

Tomazevic, M. (1999) Earthquake-resistant design of masonry buildings. *Imperial College Press, London.*

Tzamtzis, A.D., Asteris P.G., (2002). "A 3D model for non-linear microscopic FE analysis of masonry structures"*, Proceeding of the sixth international masonry conference, London, (9), pp.493-497.*

Vasconcelos G. (2005) Experimental investigations on the mechanics of stone masonry: Characterization of granites and behavior of ancient masonry shear walls. *Ph.D. dissertation. Portugal: University of Minho.*